Supporting Information

Boosting ammonia synthesis activity of ceria-supported Ru catalyst achieved through trace Pr addition

Chunyan Li[a,b], Zecheng Zhang[b], Lingyun Zhou[a], Biyun Fang[b], Jun Ni[b], Jianxin Lin[b], Bingyu Lin[b], and Lilong Jiang*[b]*

[a] Key Laboratory of Low-Dimensional Materials and Big Data, School of Chemical Engineering, Guizhou Minzu University, Guiyang 550025, China

[b] National Engineering Research Center of Chemical Fertilizer Catalyst, College of Chemical Engineering, Fuzhou University, Fuzhou 350002, Fujian, China

E-mail: bylin@fzu.edu.cn (Bingyu Lin); jll@fzu.edu.cn (Lilong Jiang); Fax: +86 0591-83738808; Tel: +86 0591-83731234

1. Preparation of Samples

The CeO_2 and Pr-doped CeO_2 with 0.1% content were prepared using the hydrothermal method. Typically, 8 mmol of $Ce(NO_3)_3$•$6H_2O$ in 20 mL distilled water was added into 1 mol NaOH aqueous solution (140 mL), and stirred at 50 ℃ for 0.5 h. The mixture solution was held at 100 °C for 24 h in an autoclave. The separated resultant product was washed with distilled water and ethanol to control the pH to neutral, dried at 60 ℃ overnight, and finally calcined at 550 ℃ for 4 h. The Pr-doped CeO_2 simple with the Pr/Ce mole ratio of 0.1% was prepared in a similar procedure.

The Ru catalysts were obtained using ruthenium nitrosyl nitrate solution (1.5% w/v) as Ru precursor by impregnation method, and the loading of Ru was fixed at 3wt%. The as-prepared simples were then reduced in 25%N_2−75%H_2 at 400 °C for 6 h and labeled as Ru/CeO_2 and Ru/PrCe.

2. Catalysts evaluation and Characterization

2.1 Catalysts evaluation

Ammonia synthesis was carried out in a continuous flow fixed-bed stainless steel reactor (inner diameter = 12 mm). Prior to reaction, the catalyst (0.2 g, 32–60 mesh) was diluted with quartz sand of similar size and reduced in a stoichiometric H_2–N_2 gas mixture at 500 °C for 6 h. There were no external and internal diffusion limitations under the conditions adopted in this work.[1, 2] Catalyst evaluation was conducted after the reaction was maintained for more than 3 h under a selected condition. The produced ammonia was trapped by sulfuric acid solution and then analyzed by ion chromatography (Thermo Scientific, ICS-600); subsequently, the reaction rates and TOF values were calculated according to the following equations:

$$\text{reaction rate} = \frac{\text{mol of } NH_4^+}{\text{mass of catalyst (g)} \times \text{time (h)}}$$

$$\text{TOF} = \frac{\text{mol of } NH_4^+}{\text{mol of metallic Ru atom} \times \text{time (s)}}$$

2.2 Catalysts Characterization

Transmission electron microscopy (TEM) and high-angle annular dark-field scanning transmission electron microscopy (HAADF-STEM) images were obtained by a FEI Tecnai G2 F30 microscope. The Brunauer–Emmett–Teller (BET) surface area, pore volume, and pore size distribution of the samples were measured with an ASAP 2020M instrument using adsorption of N_2 at 77 K. Prior to adsorption analysis, the catalysts were degassed in a flowing N_2 at 300 °C for 3 h. The phase purity and crystal structure of the catalysts were examined by X-ray diffraction (XRD, PANalytical X'Pert3 Powder diffractometer), using Cu Kα radiation (λ=0.154 32 nm). Raman spectra of samples were acquired on an InVia Reflex Raman microscope equipped with a 532 nm laser.

Diffuse reflectance infrared Fourier transform spectroscopy (DRIFTS) was measured on a Nicolet 6700 spectrometer operated at a resolution of 4 cm^{-1} with 32 scans. For CO adsorption measurements, For CO adsorption measurements of fresh catalysts, the samples were reduced in hydrogen at 500 °C for 6 h, then purged with He and cooled down to 50 ℃. After the collection of background spectrum, the

sample was exposed to 5% CO/He (50 mL/min) for 10 min. To acquire the information related to deuterium species, the sample was reduced at 500 °C in H_2 and then cooled down to 50 °C in a flow of He.

Hydrogen temperature-programmed reduction (H_2-TPR) of as-prepared catalysts was carried out on a Micromeritics AutoChem II 2920. The catalyst (100 mg, sieve fraction 0.30–0.56 mm) was pretreated in Ar at 150 °C for 60 min and then cooled to –20 °C. Afterward, the samples were heated in a flow of 10% H_2/Ar mixture (30 mL min^{-1}) to 600 °C at a rate of 10 °C min^{-1}. Temperature-programmed desorption (TPD) experiment was also performed using the same AutoChem II 2920 equipment. A sample (100 mg) was reduced in H_2 at 500 °C for 6 h, and then purged with Ar and cooled to 400 °C. Afterwards, the gas flow was switched to H_2 for sample exposure at 400 °C for 1 h. After cooling to 50 °C, the sample was purged with Ar for 1 h, and then heated to 600 °C at a rate of 10, 20 and 30 °C/min.

X-ray photoelectron spectroscopy (XPS) measurement was recorded on an ESCALAB 250Xi photoelectron spectrometer (Thermo Fisher Scientific). Charging effects were corrected by adjusting the main C 1s peak to a position of 284.6 eV. For the fresh catalysts, the sample was first reduced at 500 °C for 6 h in a flow of 5%H_2/Ar mixture (30 mL/min) in the pretreatment chamber. After cooling down to room temperature, the catalyst was transferred into the analysis chamber for XPS acquisition without exposure to air.

3 Computational details

3.1 Computational methods

Density functional theory (DFT) executed in the Vienna ab initio simulation package (VASP6.3.3) were used for all the calculations[3-6]. Exchange and correlation were treated within the Perdew-Burke-Ernzerhof (PBE) generalized gradient approximation (GGA)[7]. The valence electrons were described by a plane wave basis set with the kinetic cutoff energy of 400 eV, and the core electrons were replaced by the projector augmented wave (PAW) pseudopotentials[8, 9]. DFT + U corrections were applied to describe

the 4f orbitals of Ce and Pr with the value of U − J = 4.5 eV and 6.0 eV, respectively, which were proposed by previous works[10, 11]. The Hellman-Feynman forces on each ion were lower than 0.03 eV/Å for all the structures.

The adsorption energy (ΔE_{ads}) was given by Eq(1), in which E_{total} was the total energy of the whole system upon adsorption, E_{mol} was the energy of the gas-phase molecule, and E_{slab} was the energy of the clean slab.

$$\Delta E_{ads} = E_{total} - (E_{slab} + E_{mol}) \quad \text{Eq(1)}$$

The energy for the formation of oxygen vacancy (ΔE_{Ovac}) was calculated by Eq(2).

$$\Delta E_{Ovac} = (E_{slab\text{-}Ovac} + E_O) - E_{slab} \quad \text{Eq(2)}$$

Where E_O and $E_{slab\text{-}O}$ represented the energies of O atom and slab without the O atom.

3.2 Theoretical models

The CeO_2(111) surface was modelled by a (3×3) supercell with symmetric nine-layer, which was separated by a 15 Å vacuum layer, and a 3×3×1 Monkhorst-Pack procedure[12]. This model is equal to three stoichiometric layers of CeO_2. The Pr modified model was constructed by replacing a Ce in the top layer of CeO_2(111), denoted as $PrCeO_2$(111) (see Fig. Sx). Four-layer Ru(0001) was constructed with (3 × 3) supercell. Due to the complexity of the catalysts synthesized in the experiment, a relatively simplified model was used to decouple the role of Pr. In order to obtain data faster, we used a single Ru adsorbed on the surface before and after Pr modification to form a Ru catalyst loaded on CeO_2. We put Ru on a oxygen vacancy to get the Ru model, similar with previous work[13].

4. Mass and Heat Transfer Calculations for Ammonia Synthesis over Ru/CePr

Mass and Heat Transfer Calculations for Ammonia Synthesis on **Ru/CePr**

Mears Criterion for External Diffusion (Fogler, p841; Mears, 1971)

If $\frac{-r_A' \rho_b R n}{k_c C_{Ab}} < 0.15$, then external mass transfer effects can be neglected.

$-r_A'$ = reaction rate of nitrogen, kmol/kg-cat·s

n = reaction order with respect to N_2 (*e.g.* K. Aika et al, Appl. Catal., **28**(1986) 57–68).

R = catalyst particle radius, m

ρ_b = bulk density of catalyst bed, kg/m^3

C_{Ab} = bulk gas concentration of nitrogen, kmol/m^3

k_c = mass transfer coefficient, m/s

$\frac{-r_A' \rho_b Rn}{k_c C_{Ab}}$ =[3.3 x 10^{-6} kmol-N_2/kg-cat·s] [910 kg/m^3][3 x 10^{-4} m][1]/([1.7 m/s]*[0.045 kmol/m^3])**= 1.2x10^{-5} <0.15 {Mears for External Diffusion}**

Weisz-Prater Criterion for Internal Diffusion (Fogler, p839)

If $C_{WP} = \frac{-r'_A \rho_c R^2}{D_e C_{Ab}} < 1$, then internal mass transfer effects can be neglected.

$-r_A'$ = reaction rate of nitrogen, kmol /(kg-cat·s)

ρ_c = solid catalyst density (kg m^{-3})

R = catalyst particle radius, m

ρ_b = bulk density of catalyst bed, kg/m^3

C_{Ab} = bulk gas concentration of nitrogen, kmol/m^3

k_c = mass transfer coefficient, m/s

D_e = effective gas-phase diffusivity, m^2/s

$C_{WP} = \frac{-r'_A \rho_c R^2}{D_e C_{Ab}}$ =[3.3 x 10^{-6} kmol-N_2/kg-cat·s] × [4×10^3 kg-cat/m^3] × [3 x 10^{-4} m]^2 / ([3.34 x 10^{-6} m^2/s] × [0.045 kmol/m^3]) = **7.9x10^{-3} < 1 {Weisz-Prater Criterion for Internal Diffusion}**

Mears Criterion for External (Interphase) Heat Transfer (Fogler, p842)

$$\left|\frac{-\Delta H_r(-r_A')\rho_b RE}{h_t T_b{}^2 R_g}\right| < 0.15$$

[136.9 kJ/mol× 3.3 x 10^{-6} kmol-N_2/(kg-cat·s) × 910 kg-cat/m^3 ×3 x 10^{-4} m× 150 kJ/mol] / [185.3 kJ/m^2.K.s × 673^2 K^2× 8.314 ×10^{-3} kJ/mol.K]= 2.7x10^{-5} < 0.15 **{Mears Criterion for External (Interphase) Heat Transfer}**

Mears Criterion for Combined Interphase and Intraparticle Heat and Mass Transport (Mears, 1971)

$$\frac{-r'_A R^2}{C_{Ab} D_e} < \frac{1+0.33\gamma\chi}{|n-\gamma_b\beta_b|(1+0.33n\omega)}$$

$$\gamma = \frac{E}{R_g T_s};\quad \gamma_b = \frac{E}{R_g T_b};\quad \beta_b = \frac{(-\Delta H_r) D_e C_{Ab}}{\lambda T_b};\quad \chi = \frac{(-\Delta H_r) - r'_A R}{h_t T_b};\quad \omega = \frac{-r'_A R}{k_c C_{Ab}}$$

γ = Arrhenius number; β_b = heat generation function;

λ = catalyst thermal conductivity, W/m.K;

χ = Damköhler number for interphase heat transport

ω = Damköhler number for interphase mass transport

$\frac{-r'_A \rho_b R^2}{C_{Ab} D_e}$ =[3.3 x 10^{-6} kmol-N_2/kg-cat·s × 910 kg-cat/m^3× (3 x 10^{-4})^2 m^2]/ ([3.34 x 10^{-6} m^2/s] × [0.045 kmol/m^3])= 1.8x10^{-3}

$\frac{1+0.33\gamma\chi}{|n-\gamma_b\beta_b|(1+0.33n\omega)}$ =2.25

Left member < Right member **{Mears Criterion for Interphase and Intraparticle Heat and Mass Transport }**

Table S1 Catalytic performance of Ru-based catalysts on various supports.

Samples	Rate (μmol g^{-1} h^{-1})	TOF [a] (Ru $atom^{-1}$ s^{-1})	Reaction conditions	SV (mL g^{-1} h^{-1})	Ref.
Ru(3%)/CePr	23 500	22.6×10^{-3}	1MPa, 400 °C	36 000	This
Ru(3%)/CeO_2	16 500	15.9×10^{-3}	1MPa, 400 °C	36 000	
Ru(3%)/CePr-CO	13 000	12.5×10^{-3}	1MPa, 400 °C	36 000	
Ru(3%)/Pr_2O_3	16 800	16.2×10^{-3}	1MPa, 400 °C	36 000	
Ru(3%)/PrO_x-CeO_2	19 200	18.5×10^{-3}	1MPa, 400 °C	36 000	
Ru(3%)/CePr(0.5 mol%Pr)	18 635	18.0×10^{-3}	1MPa, 400 °C	36 000	work
Ru(3%)/Ti-Ce-S	14 580	14.1×10^{-3}	1MPa, 400 °C	36 000	14
Ru(3%)/$Ti_{0.18}$-Ce	18 912	18.7×10^{-3}	1MPa, 400 °C	36 000	15
	23 028	22.7×10^{-3}	1MPa, 400 °C	72 000	
Ba-Ru(5%)/Al_2O_3	2 796	1.7×10^{-3}	1MPa, 400 °C	36 000	16
	2 083	1.3×10^{-3}	1MPa, 400 °C	18 000	
Ru(0.25%)/CeO_2	1 950	21.9×10^{-3}	1 MPa, 400 °C	36 000	17
	2 647	29.8×10^{-3}	1 MPa, 400 °C	72 000	
Ru(3%)/CeO_2	22 075	21.3×10^{-3}	1 MPa, 400 °C	36 000	
SC-Ru(1%)/CeO_2	6 909	19.6×10^{-3}	1MPa, 400 °C	36 000	18
Ru(1%)/CeO_2-N_2H_4	5 521	15.6×10^{-3}	1MPa, 400 °C	36 000	19
Ru(1%)/CeO_2-BH	5 454	15.4×10^{-3}	1 MPa, 400 °C	36 000	20
Ru(3%)/$Ti_{0.18}$-Ce	18 912	18.7×10^{-3}	1MPa,400°C	36 000	
Ru(10%)/Ba-$Ca(NH_2)_2$	50 000	14.0×10^{-3}	0.9MPa,400°C	36 000	21
Ru(6%)-Cs/MgO	23 000	6.5×10^{-3}	0.9MPa,360°C	36 000	
Ru(10%)/Ba-$Ca(NH_2)_2$	60 400	16.9×10^{-3}	1 MPa, 400 °C	36 000	
Ru(9.1%)-Ba/AC	8 285	2.6×10^{-3}	1 MPa, 400 °C	18 000	22
Ru(6%)-Cs/MgO	12 117	5.7×10^{-3}	1 MPa, 400 °C	18 000	
Ru(4%)/$C_{12}A_7$:e^-	6 089	4.3×10^{-3}	1 MPa, 400 °C	18 000	
Ru(7.8%)/Y_5Si_3	4 100	1.5×10^{-3}	1 MPa, 400 °C	18 000	23
Ru(4%)/r-CeO_2	3 830	2.7×10^{-3}	1 MPa, 400 °C	18 000	24

Ru(4%)/c-CeO_2	1 289	0.9×10^{-3}	1 MPa, 400 °C	18 000	
Ru(4%)/p-CeO_2	529	0.4×10^{-3}	0.9MPa,400°C	18 000	
Ru(5%)/CeO_2	7 200	4.0×10^{-3}	0.9MPa,400°C	18 000	[25]
Ru(5%)/MgO	1 800	1.0×10^{-3}	0.1MPa,400°C	18 000	
Ru(1.8%)/LaScSi	28 00	$\times10^{-3}$	1 MPa, 400 °C	18 000	
Ba-Ru(5%)/Al_2O_3-980	7 217	4.5×10^{-3}	5 MPa, 400 °C	60 000	[26]
Cs-Ru(1%)/MgO	2 700	1.0×10^{-3}	5 MPa, 400 °C	66 000	[27]
Ru(1%)/$BaTiO_3$	4 100	1.5×10^{-3}	1 MPa, 400 °C	66 000	
Ru(5%)/$La_{0.5}Ce_{0.5}O_{1.75}$	65 000	36.5×10^{-3}	1 MPa, 400 °C	72 000	[28]
Ru(5%)/$La_{0.5}Pr_{0.5}O_{1.75}$	60 200	33.8×10^{-3}	1 MPa, 400 °C	72 000	[29]

[a] based on total number of Ru atoms

Table S2 The compositions of Ru catalysts obtained from ICP analysis.

Sample	Pr (wt.%)	Ru (wt.%)	
		Theoretical value (wt. %)	Actual value (wt. %)
Ru/CeO_2	--	2.90	2.40
Ru/CePr	0.08		2.35

Table S3 Textural properties of Ru catalysts with different reduction conditions.

Samples	Surface area ($m^2\ g^{-1}$)	Pore volume ($cm^3 g^{-1}$)	Average pore size (nm)
CeO_2	71	0.3	17
CePr	79	0.4	19
Ru/CeO_2	63	0.3	20
Ru/CePr	63	0. 4	24

Table S4 Binding energies and FWHM of the C 1s, O 1s, Ce $3d_{5/2}$ and Ru $3d_{5/2}$ regions for Ru catalysts determined by XPS

Region	Ru/CeO_2		Ru/CePr	
	Binding energy	FWHM	Binding energy	FWHM
C 1s	284.60	1.14	284.60	1.14
	285.25	1.72	285.42	1.65
	289.04	3.07	289.09	3.15
Ru $3d_{5/2}$	279.62	0.91	279.54	0.91
	280.25	1.44	280.31	1.44
	282.69	1.94	282.74	1.94
O 1s	529.15	1.12	529.15	1.04
	531.03	1.50	531.22	1.52
Ce $3d_{5/2}$	880.60	2.44	880.62	2.44
	884.57	3.50	884.78	3.50
	882.27	1.62	882.27	1.62
	888.81	3.50	888.76	3.50
	898.10	2.08	898.08	2.08

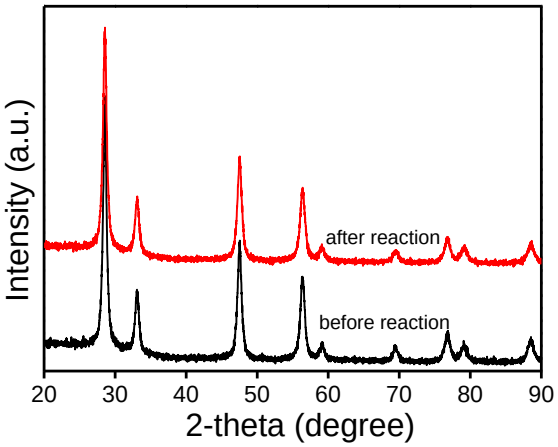

Fig. S1 XRD patterns of Ru/CePr catalyst.

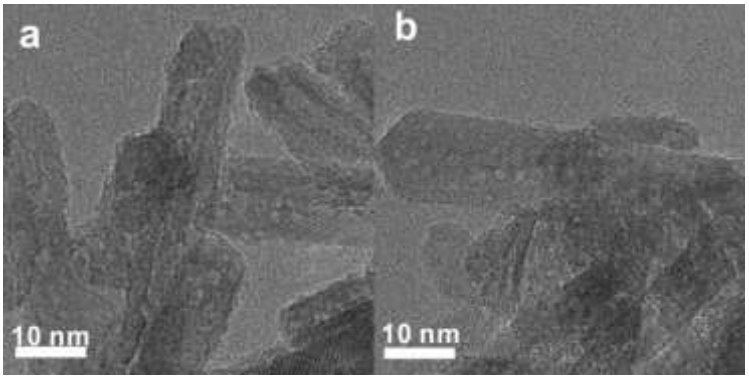

Fig. S2 HRTEM images of Ru/CePr catalyst (a) before reaction and (b) after reaction.

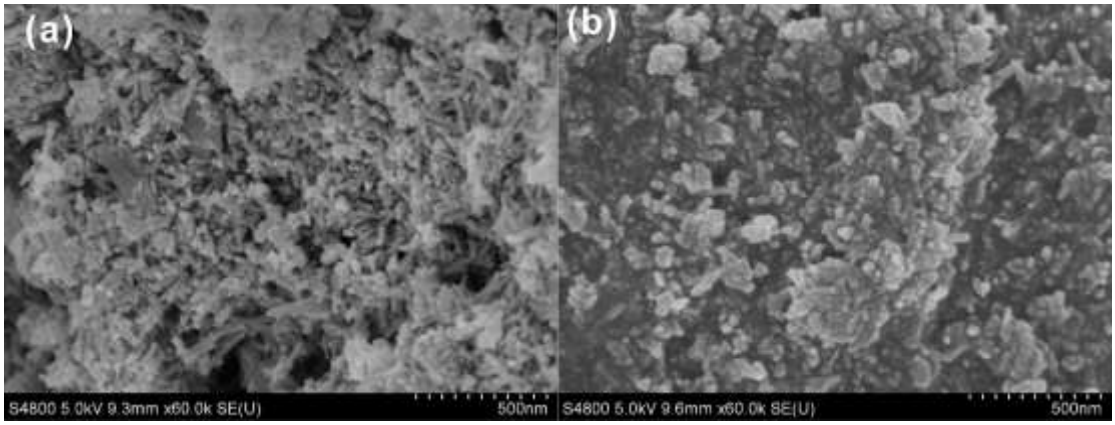

Fig. S3 SEM images of (a) Ru/CeO_2 and (b) Ru/CePr.

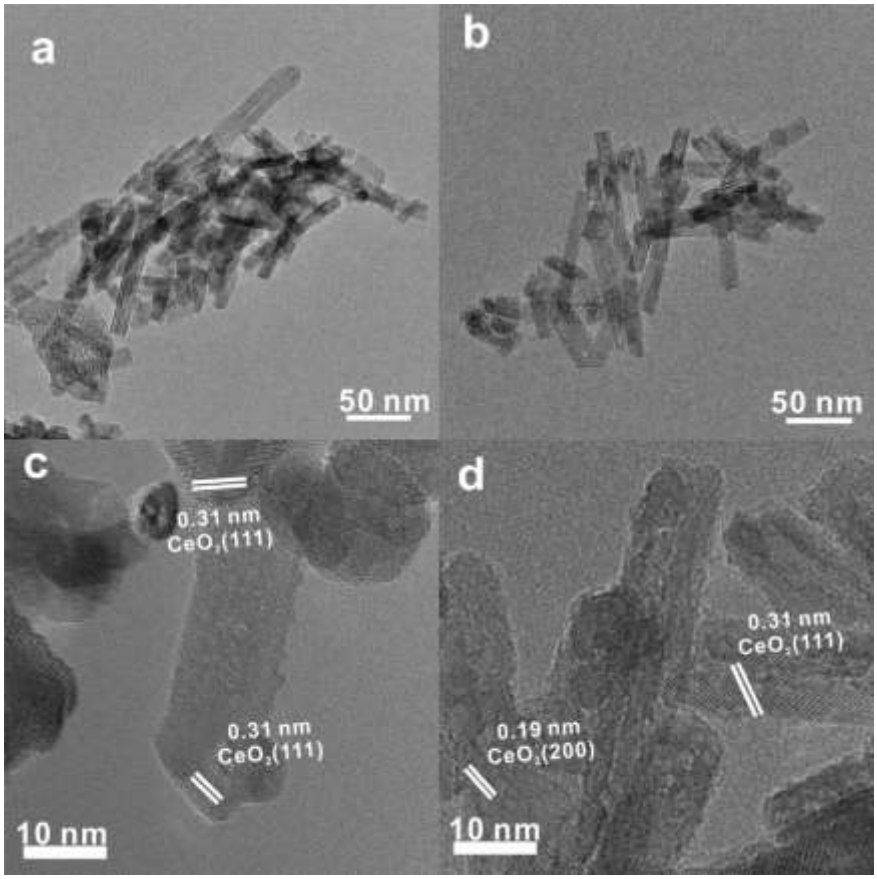

Fig. S4 TEM images of (a, c) Ru/CeO_2 and (b, d) Ru/CePr.

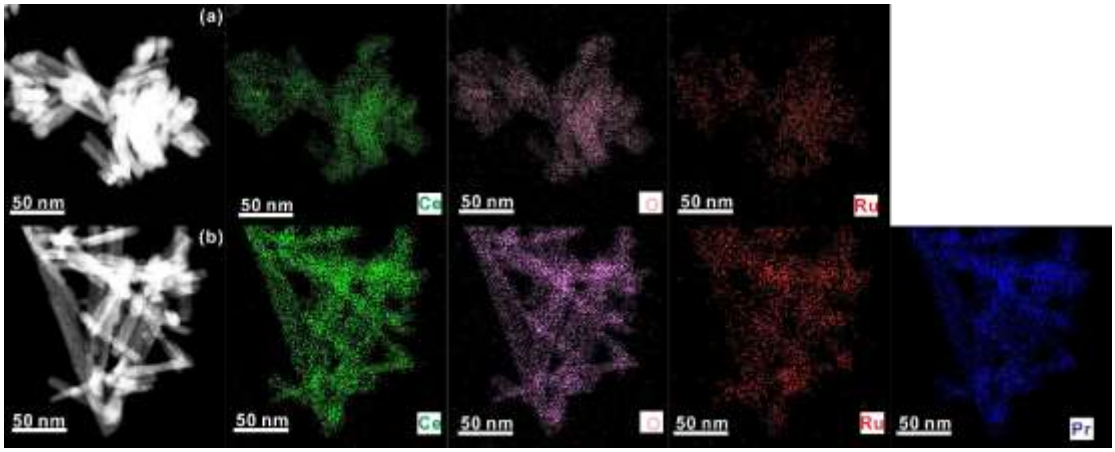

Fig. S5 HAADF-STEM elemental mapping of (a) Ru/CeO_2 and (b) Ru/CePr.

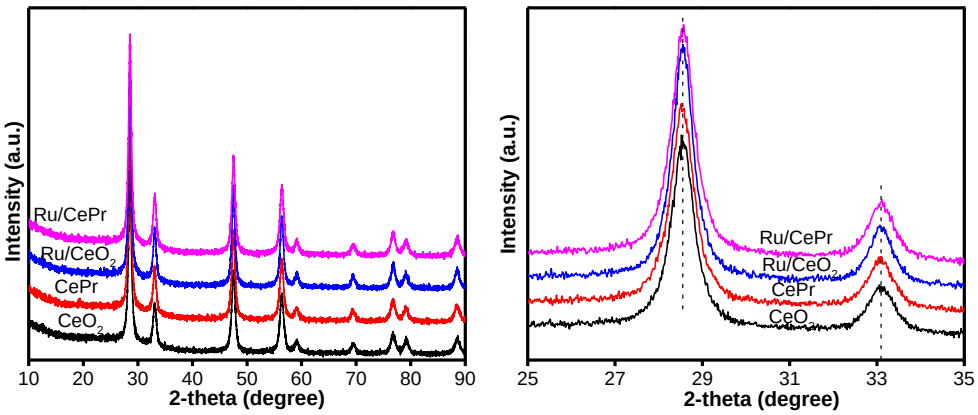

Fig. S6 XRD patterns of supports and Ru catalysts.

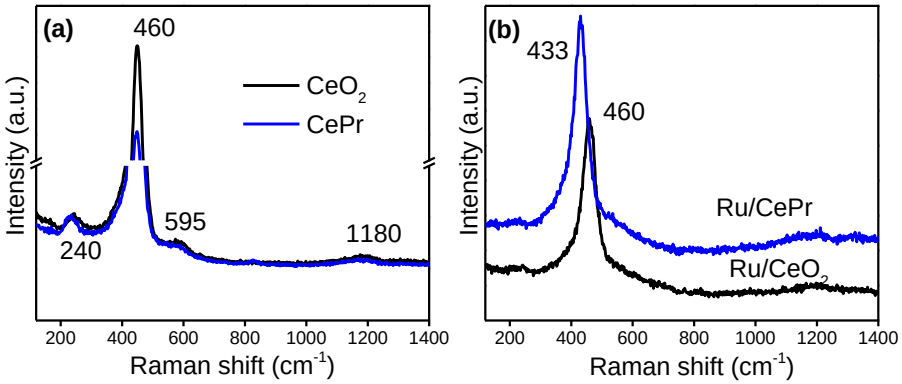

Fig. S7 Raman spectra of (a) supports and (b) Ru catalysts.

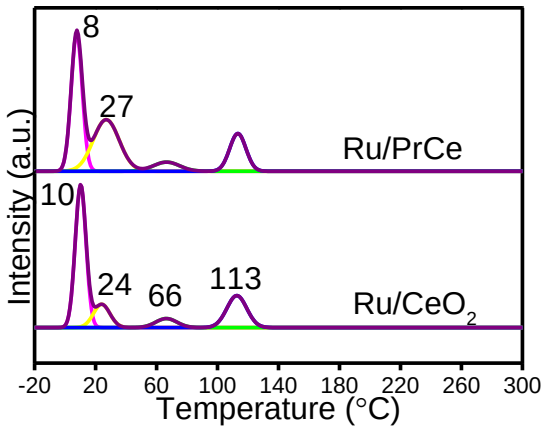

Fig. S8 H_2-TPR profiles of the samples with oxidization in oxygen at 150 °C.

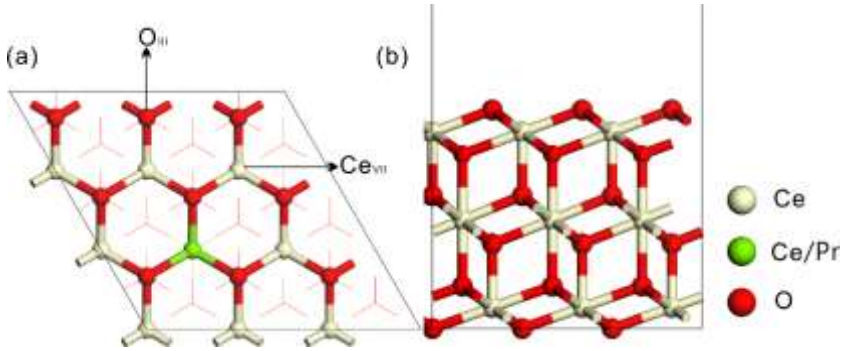

Fig. S9. Top view (a) and side view (b) of the CeO_2(111) surface with or without Pr modification.

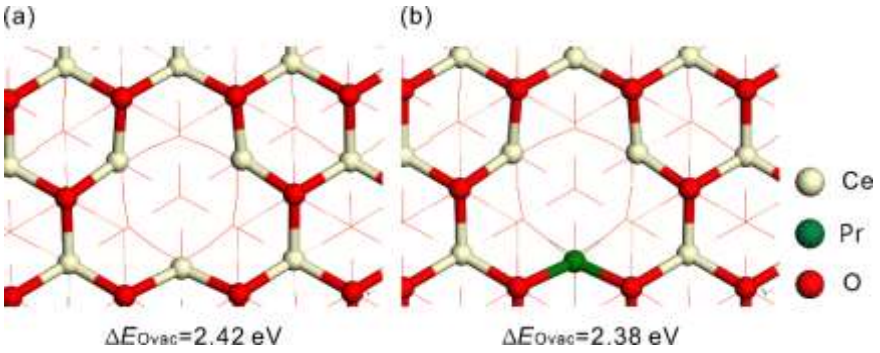

Fig. S10. Top view of the slab with one oxygen vacancy and its formation energy. (a) $CeO_2(111)$, (b) $PrCeO_2(111)$.

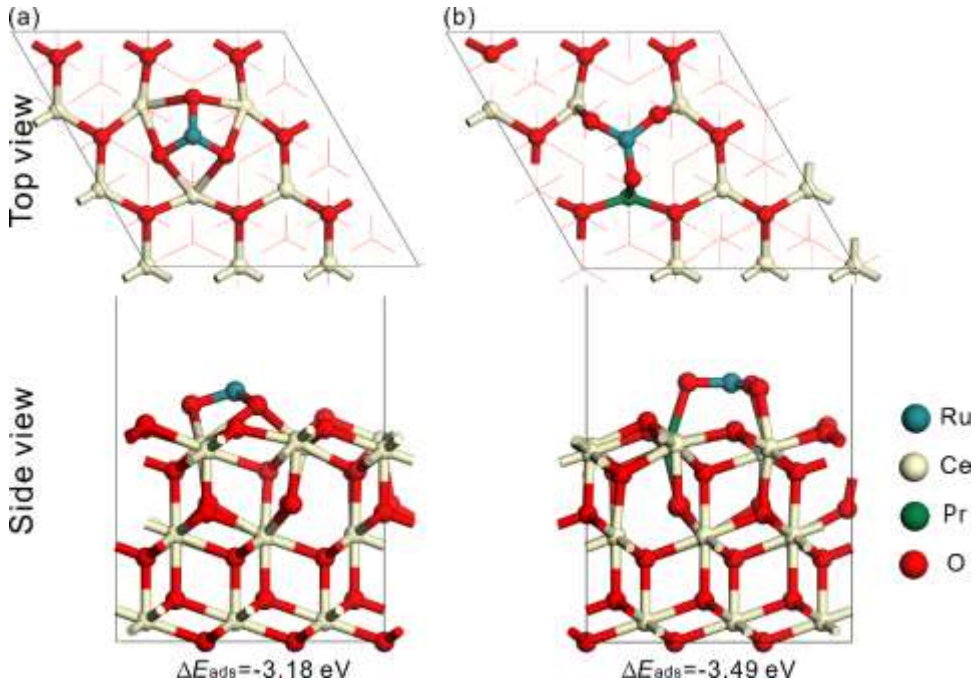

Fig. S11. Top view and side view of the Ru/CeO_2 (111) surface without or with Pr modification. (a) Ru/CeO_2 (111), (b) Ru/$PrCeO_2$ (111).

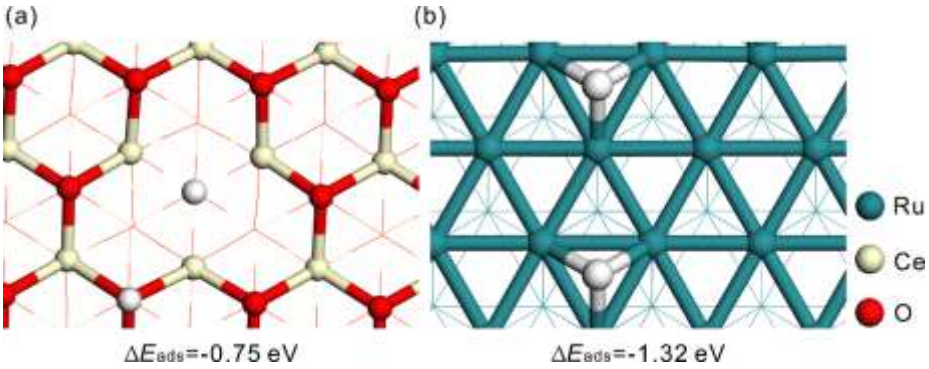

Fig. S12. The optimized structures of H_2 on CeO_2 (111) with oxygen vacancy (a) and (b) Ru(0001).

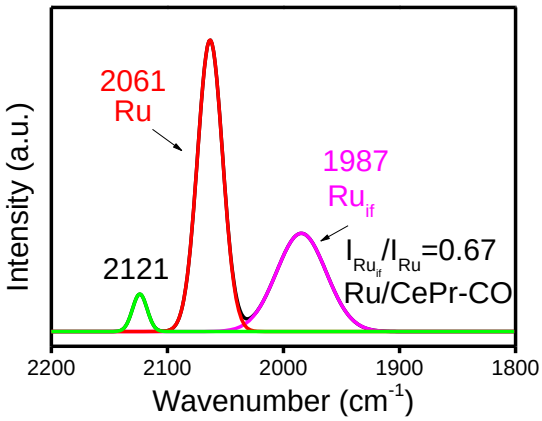

Fig. S13 The CO-IR spectra of Ru/CePr-CO catalyst.

References

1. Oyama, S. T.; Zhang, X.; Lu, J.; Gu, Y.; Fujitani, T., Epoxidation of propylene with H_2 and O_2 in the explosive regime in a packed-bed catalytic membrane reactor. *J. Catal.* **2008,** *257* (1), 1–4.
2. Mears, D. E., Tests for Transport Limitations in Experimental Catalytic Reactors. *Industrial & Engineering Chemistry Process Design and Development* **1971,** *10* (4), 541–547.
3. Kresse, G.; Hafner, J., Ab initio molecular-dynamics simulation of the liquid-metal--amorphous-semiconductor transition in germanium. *Phys. Rev. B* **1994,** *49* (20), 14251-14269.
4. Kresse, G.; Hafner, J., Ab initio molecular dynamics for open-shell transition metals. *Phys. Rev. B* **1993,** *48* (17), 13115-13118.
5. Kresse, G.; Furthmüller, J., Efficiency of ab-initio total energy calculations for metals and semiconductors using a plane-wave basis set. *Comp. Mater. Sci.* **1996,** *6* (1), 15-50.
6. Kresse, G.; Furthmüller, J., Efficient iterative schemes for ab initio total-energy calculations using a plane-wave basis set. *Phys. Rev. B* **1996,** *54* (16), 11169-11186.
7. Kresse, G.; Hafner, J., Ab initio molecular dynamics for liquid metals. *Phys. Rev. B* **1993,** *47* (1), 558-561.
8. Kresse, G.; Joubert, D., From ultrasoft pseudopotentials to the projector augmented-wave method. *Phys. Rev. B* **1999,** *59* (3), 1758-1775.
9. Kresse, G.; Hafner, J., Ab initio molecular dynamics for open-shell transition metals. *Phys. Rev. B* **1993,** *48* (17), 13115-13118.
10. Capdevila-Cortada, M.; García-Melchor, M.; López, N., Unraveling the structure sensitivity in methanol conversion on CeO_2: A DFT+ U study. *J. Catal.* **2015,** *327*, 58-64.
11. Tran, F.; Schweifer, J.; Blaha, P.; Schwarz, K.; Novák, P., PBE+ U calculations of the Jahn-Teller effect in PrO_2. *Physical Review B* **2008,** *77* (8), 085123.
12. Monkhorst, H. J.; Pack, J. D., Special points for Brillouin-zone integrations. *Phys. Rev. B* **1976,** *13* (12), 5188-5192.
13. Tang, Y.; Zhao, S.; Long, B.; Liu, J.-C.; Li, J., On the Nature of Support Effects of Metal Dioxides MO2 (M = Ti, Zr, Hf, Ce, Th) in Single-Atom Gold Catalysts: Importance of Quantum Primogenic Effect. *J. Phys. Chem. C* **2016,** *120* (31), 17514-17526.
14. Wu, Y.; Li, C.; Fang, B.; Wang, X.; Ni, J.; Lin, B.; Lin, J.; Jiang, L., Enhanced Ammonia Synthesis Performances of Ceria-supported Ru Catalysts via Introduction of Titanium. *Chem. Commun.*
15. Li, C.; Zhang, Z.; Zheng, Y.; Fang, B.; Ni, J.; Lin, J.; Lin, B.; Wang, X.; Jiang, L., Titanium modified Ru/CeO_2 catalysts for ammonia synthesis. *Chem. Eng. Sci.* **2022,** *251*, 117434.
16. Lin, B.; Heng, L.; Yin, H.; Fang, B.; Ni, J.; Wang, X.; Lin, J.; Jiang, L., Effects of Using Carbon-Coated Alumina as Support for Ba-Promoted Ru Catalyst in Ammonia Synthesis. *Ind. Eng. Chem. Res.* **2019,** *58* (24), 10285-10295.
17. Lin, B.; Wu, Y.; Fang, B.; Li, C.; Ni, J.; Wang, X.; Lin, J.; Jiang, L., Ru surface density effect on ammonia synthesis activity and hydrogen poisoning of ceria-supported Ru catalysts. *Chin. J. Catal.* **2021,** *42* (10), 1712–1723.
18. Fang, B.; Liu, F.; Zhang, C.; Li, C.; Ni, J.; Wang, X.; Lin, J.; Lin, B.; Jiang, L., Sacrificial Sucrose Strategy Achieved Enhancement of Ammonia Synthesis Activity over a Ceria-Supported Ru Catalyst. *ACS Sustain. Chem. Eng.* **2021,** *9* (27), 8962–8969.
19. Li, C.; Liu, F.; Shi, Y.; Zheng, Y.; Fang, B.; Lin, J.; Ni, J.; Wang, X.; Lin, B.; Jiang, L., Inducing the Metal–Support Interaction and Enhancing the Ammonia Synthesis Activity of Ceria-Supported

Ruthenium Catalyst via N_2H_4 Reduction. *ACS Sustain. Chem. Eng.* **2021,** *9* (13), 4885–4893.

20. Li, C.; Shi, Y.; Zhang, Z.; Ni, J.; Wang, X.; Lin, J.; Lin, B.; Jiang, L., Improving the ammonia synthesis activity of Ru/CeO_2 through enhancement of the metal–support interaction. *J. Energy Chem.* **2021,** *60*, 403-409.

21. Kitano, M.; Inoue, Y.; Sasase, M.; Kishida, K.; Kobayashi, Y.; Nishiyama, K.; Tada, T.; Kawamura, S.; Yokoyama, T.; Hara, M.; Hosono, H., Self-organized Ruthenium–Barium Core–Shell Nanoparticles on a Mesoporous Calcium Amide Matrix for Efficient Low-Temperature Ammonia Synthesis. *Angew. Chem. Int. Edit.* **2018,** *57* (10), 2648–2652.

22. Kitano, M.; Inoue, Y.; Yamazaki, Y.; Hayashi, F.; Kanbara, S.; Matsuishi, S.; Yokoyama, T.; Kim, S.-W.; Hara, M.; Hosono, H., Ammonia synthesis using a stable electride as an electron donor and reversible hydrogen store. *Nat. Chem.* **2012,** *4* (11), 934–940.

23. Lu, Y.; Li, J.; Tada, T.; Toda, Y.; Ueda, S.; Yokoyama, T.; Kitano, M.; Hosono, H., Water Durable Electride Y_5Si_3: Electronic Structure and Catalytic Activity for Ammonia Synthesis. *J. Am. Chem. Soc.* **2016,** *138* (12), 3970–3973.

24. Ma, Z.; Zhao, S.; Pei, X.; Xiong, X.; Hu, B., New insights into the support morphology-dependent ammonia synthesis activity of Ru/CeO_2 catalysts. *Catal. Sci. Technol.* **2017,** *7* (1), 191-199.

25. Sato, K.; Imamura, K.; Kawano, Y.; Miyahara, S.-i.; Yamamoto, T.; Matsumura, S.; Nagaoka, K., A low-crystalline ruthenium nano-layer supported on praseodymium oxide as an active catalyst for ammonia synthesis. *Chem. Sci.* **2017,** *8* (1), 674–679.

26. Lin, B.; Heng, L.; Fang, B.; Yin, H.; Ni, J.; Wang, X.; Lin, J.; Jiang, L., Ammonia Synthesis Activity of Alumina-Supported Ruthenium Catalyst Enhanced by Alumina Phase Transformation. *ACS Catal.* **2019,** *9* (3), 1635–1644.

27. Kobayashi, Y.; Tang, Y.; Kageyama, T.; Yamashita, H.; Masuda, N.; Hosokawa, S.; Kageyama, H., Titanium-Based Hydrides as Heterogeneous Catalysts for Ammonia Synthesis. *J. Am. Chem. Soc.* **2017,** *139* (50), 18240–18246.

28. Ogura, Y.; Sato, K.; Miyahara, S.-i.; Kawano, Y.; Toriyama, T.; Yamamoto, T.; Matsumura, S.; Hosokawa, S.; Nagaoka, K., Efficient ammonia synthesis over a Ru/$La_{0.5}Ce_{0.5}O_{1.75}$ catalyst pre-reduced at high temperature. *Chem. Sci.* **2018,** *9* (8), 2230–2237.

29. Ogura, Y.; Tsujimaru, K.; Sato, K.; Miyahara, S.-i.; Toriyama, T.; Yamamoto, T.; Matsumura, S.; Nagaoka, K., Ru/$La_{0.5}Pr_{0.5}O_{1.75}$ Catalyst for Low-Temperature Ammonia Synthesis. *ACS Sustain. Chem. Eng.* **2018,** *6* (12), 17258-17266.